I&EC research
Industrial & Engineering Chemistry Research
pubs.acs.org/IECR
Article

Accelerating Electro-oxidation Turnover Rates via Potential-Modulated Stimulation of Electrocatalytic Activity

Alex M. Román, Taylor D. Spivey, J. Will Medlin, and Adam Holewinski*

Cite This: *Ind. Eng. Chem. Res.* 2020, 59, 19999−20010

ABSTRACT: Herein, we describe a method of potential-modulated stimulation of electrocatalytic activity (PSEA) and apply it to the electro-oxidation of formic acid in acidic (pH 1) electrolyte. Ordinarily, the reaction shows a rapid decay in steady-state current as a consequence of the accumulation of strongly bound adsorbates. PSEA leads to a high resilience against deactivation and an overall enhancement in rate. Results showed an ∼30-fold increase in activity, compared to the reaction under similar potentiostatic conditions after a 1-h reaction period, with further improvement likely possible by optimizing the amplitude, frequency, shape, and bounds of the applied potential waveform. A microkinetic model was adapted to further probe the underlying mechanism responsible for the shift in activity; the resulting electrocatalytic cycle was found to not simply clear the surface of strongly bound species and provide a high proportion of free sites for the "direct" formic acid oxidation pathway (major route), but also to accelerate pathways thought to be less dominant under potentiostatic conditions.

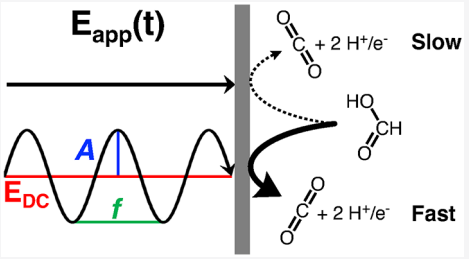

INTRODUCTION

The mechanism for the electro-oxidation of formic acid has been studied for almost 40 years. The outcome has been the discernment of the so-called "triple pathway" mechanism (Scheme 1) emanating from a large body of observations from conventional electrochemical studies, IR spectroscopy, and quantum calculations that support possibilities of three major oxidation routes.[1] The fastest reaction pathway is believed to be the so-called "direct" pathway. Several studies suggest that this pathway is highly dependent on the pH of the solution, with its maximum rate observed to plateau above the pK_A of formic acid; as a result, it is believed to involve the facile, direct activation of $CHOO^-$.[2−4] However, since the direct pathway requires available Pt sites, it becomes less operative as the surface accumulates other adsorbates.

Past attenuated total reflectance−infrared (ATR-IR) studies have indicated that formic acid initially adsorbs, and then is subsequently deprotonated, on the Pt surface, forming a bridging or bidentate conformation.[2,5,6] As "bridge-bound" formate (FA_B^*) is produced, some portion reorients (facilitated by neighboring vacant sites) to a monodentate conformation that is more favorable. This "linearly bound" formate (FA_L^*) can then either be oxidized to CO_2 via the "formate" pathway or undergo a reduction step to CO*, which can then be oxidized at sufficiently high potentials via the "indirect" pathway.

Perhaps unexpectedly, potentials that show high apparent steady-state production of CO_2 ($E \approx 0.6$ V_{RHE}, where the reaction rate is highest at pH 1) also allow a significant reduction pathway to CO* as a nearly terminal product. Once formed, the CO* remains adsorbed on the Pt surface and is only able to be oxidized to CO_2 at sufficiently high potentials where water oxidation to OH* can occur. CO does not otherwise desorb in any measurable quantity. This presents a challenge to operating under potentiostatic conditions because the potential must be sufficiently high to limit the amount of blocking CO*, but low enough to limit the amount of blocking OH*. As a consequence of this balance, the true steady state is actually unstable, and slow galvanodynamic sweeps during formic acid oxidation have been shown to result in a natural oscillatory behavior in the measured potential on Pt electrodes.[7,8] This oscillation is thought to result from the so-called "hidden negative differential resistance" attributed to a combination of potential-dependent processes that include (i) a fast process that is dependent on the availability of free surface sites (the "direct" pathway), (ii) a slower process that results in strongly bound intermediates that block sites for process (i) (adsorption of CO*), and (iii) a fast process that occurs on a time scale comparable to that of the potential oscillations (adsorption/desorption of OH*, facilitating reactive removal of CO* followed by a return to a low-coverage surface).[7] Therefore, it stands to reason that the net rate of formic acid oxidation could be accelerated using PSEA (i.e., intentional, driven oscillation) by taking advantage of the fast potential-dependent OH adsorption/desorption kinetics on Pt in order to remove CO* as quickly as it is formed. This

Received: September 8, 2020
Revised: October 25, 2020
Accepted: October 26, 2020
Published: November 3, 2020

https://dx.doi.org/10.1021/acs.iecr.0c04414
Ind. Eng. Chem. Res. 2020, 59, 19999−20010

Scheme 1. Proposed Triple-Pathway for the Electro-oxidation of Formic Acid on Pt

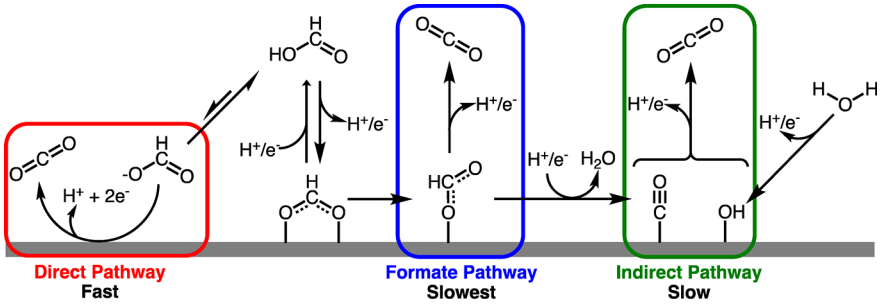

Scheme 2. Examples of General Electrocatalytic Reaction Networks That Could Be Accelerated Using PSEA To Optimize (a) the Surface Coverages of Critical Intermediates (e.g., Oxidation) and (b) the Double-Layer Concentration of Intermediates (e.g., Reduction)

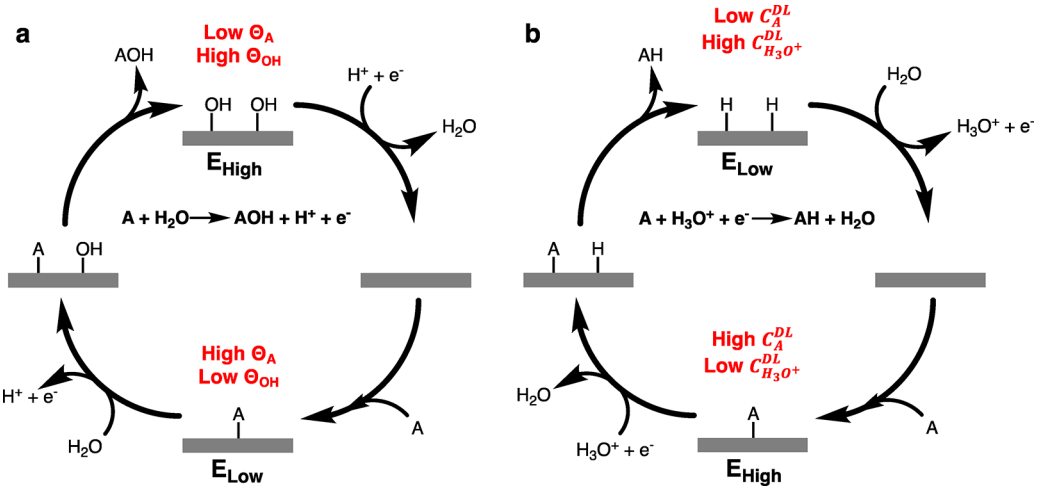

"surface clearing" must occur while simultaneously maintaining a sufficiently oxidizing potential for the direct pathway to remain favorable, while not being so high as to oversaturate the Pt surface with OH*.[9] Assuming that the ideal periodic waveform, amplitude, and frequency could be identified, the resulting Pt catalyst would be effectively resistant to deactivation via intermediate "poisoning" and could theoretically produce high rates of formic acid oxidation (although possibly at the expense of other complications, such as accelerated nanoparticle ripening, which is beyond the scope of this study).[10,11]

Related to this idea, several recent works have suggested that reactions involving heterogeneous catalysts have the potential to exceed intrinsic activities, normally maximized under the Sabatier principle, via dynamic modulation of the adsorption strength of surface-bound intermediates.[12,13] The basis of this concept is that by rapidly altering conditions at the catalyst surface between those that favor adsorption and desorption, both processes can proceed faster than the maximum steady state under fixed conditions. Electrocatalysis presents a unique opportunity to experimentally probe this concept, as an electrochemical potential can be dynamically applied to modulate the relative binding energy of reactive surface species.[14] The potential-modulated stimulation of electrocatalytic activity (PSEA) describes a myriad of techniques than can be applied to various surface-mediated electrochemical reactions in the pursuit of surpassing the inherent activity, selectivity, and/or stability exhibited under similar potentiostatic conditions. Generalized examples where various forms of PSEA have been successfully utilized are summarized in Scheme 2 and are discussed below.

Pulsed-potential electrolysis has been historically utilized as an electroanalytical tool for understanding the kinetics and mechanisms of various electrochemical reaction systems, as well as for increasing their rates.[15−18] An example of a pulse cycle for an oxidation is shown in Scheme 2 a, for which a notable example can be found in the work of Fedkiw et al. on methanol electro-oxidation. They found that the power output of a direct methanol fuel cell (DMFC) could be increased by periodically applying high overpotentials (1.4 V_{RHE}) at short time intervals in order to effectively clear the Pt electrode surface of CO*, which typically deactivates the catalyst by accumulating at desired (lower) operating potentials.[11,19−21] The CO* was quickly removed as a result of the electrogeneration of reactive OH* species and the correspondingly high oxidative driving force found at large overpotentials. The applied potential was then reduced to either 0.4 or 0.6 V, where methanol oxidation in DMFCs would conventionally operate, until the surface was once again blocked by CO* and the pulsing cycle was repeated. Even accounting for the time spent at high potentials where no power is produced, the time-averaged power output of methanol oxidation surpassed conventional potentiostatic operation by more than 2 orders of magnitude.

In contrast to "surface clearing" applications, PSEA has also been used to counteract the slow mass transfer of reactants to the electrode surface, often encountered during organic electroreduction in aqueous media (Scheme 2b). The high overpotentials needed in many electroreduction reactions can

https://dx.doi.org/10.1021/acs.iecr.0c04414
Ind. Eng. Chem. Res. 2020, 59, 19999−20010

result in a steep concentration gradients of organic reactants near the electrode surface.[22] This decrease of organic reactants near the surface allows parasitic side reactions (e.g., hydrogen evolution) to occur, decreasing the overall energy efficiency and Faradaic yield of desired product. By inducing periods where little electroreduction occurs, the amount of organic near the electrode surface returns to bulk concentration, resulting in a higher surface coverage of reactant ready to be reduced. This concept was recently studied in the electrohydrodimerization of acrylonitrile to adiponitrile.[22] Because of the complexity of the mechanism, the systematic testing of reaction variables was combined with an artificial neural network to predict an optimal operating condition—cycling between a cathodic pulse for 120 ms and a resting pulse, i.e., no applied voltage, for 5 ms. The condition was successfully found to yield 20% higher activity and 325% higher selectivity for adiponitrile versus propionitrile, compared to conventional potentiostatic operation in the same flow cell. Other effective applications of PSEA have included increasing the selectivity to desired products in the partial oxidations of furans,[23] developing potential-control algorithms for maintaining the activity of hydrogen fuel cells with CO contamination present in the H_2 feed,[24,25] and improving the activity and selectivity for the electroreduction of nitrobenzene to *p*-aminophenol in a parallel-plate flow cell model.[26]

Although several of the publications mentioned above include kinetic models to further understand and optimize the pulsed-potential applications, few models have been developed to directly address the dynamics of active surface species, or particularly to investigate how coverages can be optimally modulated with various applied potential waveforms. The electro-oxidation of formic acid on Pt electrodes in acid medium provides a simple and moderately well-understood platform for probing how the coverage of strongly bound reaction intermediates (e.g., CO*) can be controlled and optimized using potential-modulation techniques. Adzic et al. investigated this idea in the late 1970s, using pulsation of potential at high frequencies (10−10 000 Hz) centered at a few potentials, but only examined an amplitude of 600 mV.[27] A microkinetic model (MKM) was developed in this work to understand the mechanism, and since then, a number of more encompassing MKMs have been developed to describe the mechanisms of formic acid electro-oxidation on Pt. Fitting parameters for these models have been derived from conventional electrochemical experiments,[7,8,28] attenuated total reflectance surface-enhanced infrared absorption spectroscopy (ATR-SEIRAS) infrared spectroscopy,[2,4−6] and density-functional theory (DFT) calculations.[29] Given the broad range of prior work, we do not attempt to independently explore parameter estimation and statistical evaluation of the model, but we refer the reader to thoughtful tutorials on this topic for consideration of model validation.[30] In the present work, rotating disk chronoamperometry experiments on Pt electrodes are used to probe the mechanisms by which PSEA can increase the net oxidation rate of formic acid. We find an ∼30-fold increase in activity possible versus comparable potentiostatic experiments, with high resistance to deactivation. A microkinetic model is employed to understand how the surface coverages of various intermediates are impacted by the modulated potential and to provide insight into which mechanistic pathways contribute to the observed increase in turnover frequency (TOF). Our findings suggest that, while keeping the Pt surface clear of strongly bound intermediates does accelerate the dominant direct pathway, oxidation rates through the formate and indirect pathways also increase.

EXPERIMENTAL AND MODELING METHODS

Materials. All solutions were prepared using ultrapure (UP) deionized water (>18.2 MΩ cm, Millipore). All reagents and standards were used as delivered: Suprapure perchloric acid (70%, MilliporeSigma), Pt gauze (Alfa Aesar), argon (UHP, Air-Gas), and formic acid (>95%, Sigma−Aldrich).

Rotating Disk Chronoamperometry. Electrochemical experiments were conducted in a rotating disc electrode (RDE) half-cell, with a polycrystalline Pt working electrode (Pine Research), a Pt mesh counter electrode (Alfa Aesar), and a double-junction Ag/AgCl reference electrode, which was calibrated to the reversible hydrogen electrode (RHE) scale prior to experimentation. Therefore, all potentials are reported vs RHE and all reported currents are not *iR*-corrected. The Pt disc working electrode was mechanically polished using progressively finer alumina slurries (5, 0.3, 0.05 μm) followed by sonication in DI water for 20 min prior to use. Rotation of the working electrode was controlled with a modulated speed rotator (Pine Instrument Company), and electrochemical measurements were taken on a Gamry Reference 3000 potentiostat (Gamry Instruments). All experiments were conducted in argon-saturated 0.1 M $HClO_4$ (sparging/blanketing flow rate of 100 sccm). Perchloric acid was chosen as the electrolyte, because of its relatively weak anion adsorption at oxidizing potentials, compared to alternatives such as sulfuric acid, which has been shown to alter formic acid oxidation behavior at high potentials.[8]

The break-in procedure consisted of cycling the catalyst from 0.1−1.5 at 1 V/s for 500 cycles prior to use. The electrochemical surface area (ECSA) was determined to be 0.4 cm^2 (roughness factor of ∼2) during static (no rotation) cyclic voltammograms in the range of hydrogen adsorption (0.05−0.4 V at 20 mV/s) on the Pt surface, assuming a stripping charge of 210 $\mu C\ cm_{Pt}^{-2}$. After break-in and ECSA determination, 0.1 M formic acid was added to the cell, which was then resparged with argon and blanketed during the experiment. The working electrode rotation rate was set to 2500 rpm to limit interference from bubble formation due to gas (H_2, O_2, CO_2) evolution that might onset within the oscillatory window.

Microkinetic Model. The microkinetic model (MKM) is adapted from Calderón-Cárdenas et al. to include effects from a diffusion layer near the Pt RDE tip and is summarized in Scheme 3.[1] The model was solved numerically in Python using the SciPy library,[31,32] and all parameter values are given in Table 1. Oscillation calculations were run for at least 100 cycles under all

Scheme 3. Microkinetic Model Network for the Electro-oxidation of Formic Acid on Pt[a]

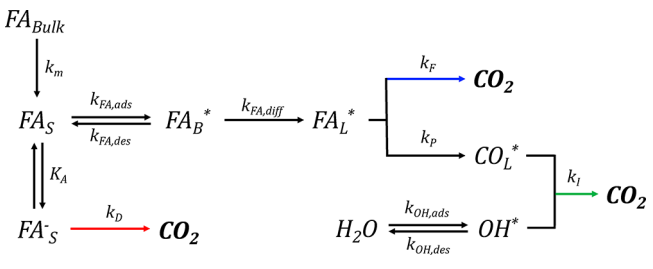

[a]Adapted from ref 1.

https://dx.doi.org/10.1021/acs.iecr.0c04414
Ind. Eng. Chem. Res. 2020, 59, 19999−20010

Table 1. Model Parameter Values[a]

parameter	value
ϕ_D	−0.4 V
$\phi_{FA,ads}$	−0.04 V
$\phi_{FA,des}$	0.02 V
ϕ_F	0.38 V
ϕ_P	0.6 V
ϕ_I	0.78 V
$\phi_{OH,ads}$	0.4 V
$\phi_{OH,des}$	0.71 V
$k_{FA,diff}$	110 s^{-1}
K_A	$1.8 \times 10^{(pH-4)}$
k_m	2.5×10^{-5} cm^2/s
$C_{FA_{Bulk}}$	0.1 mol/cm^3
C_{H_2O}	55.5 mol/cm^3
δ[8]	1.34×10^{-3} cm (2500 rpm)
S_{TOT}	2.18×10^{-9} mol Pt sites/cm^2
$\beta_{OH,ads}$	0.65
$\beta_{OH,des}$	−0.35
C_{DL}	40 $\mu F/cm^2$

[a]Taken from ref 1, except where cited otherwise.

conditions probed, which was the minimum necessary to achieve stable oscillation responses independent of initial conditions, and results were averaged from the final 10 cycles.

Each of the reaction steps in the proposed reaction network for formic acid electro-oxidation on Pt (Scheme 3) can be represented by the following chemical equations, where the asterisk symbol (*) represents vacant Pt surface sites and subscripts indicate near-surface (S), bridge-bonded (B), or linearly bonded (L) adsorbates:

$$FA_{Bulk} \xrightarrow{k_m} FA_S \quad (r1)$$

$$FA_S + 2* \underset{k_{FA,des}}{\overset{k_{FA,ads}}{\rightleftharpoons}} FA_B + H^+ + e^- \quad (r2)$$

$$FA_B + 2* \xrightarrow{k_{FA,diff}} FA_L + 3* \quad (r3)$$

$$FA_L + * \xrightarrow{k_F} CO_2 + H^+ + e^- + 2* \quad (r4)$$

$$FA_L + H^+ + e^- + 2* \xrightarrow{k_P} CO_L + H_2O + 2* \quad (r5)$$

$$H_2O + * \underset{k_{OH,des}}{\overset{k_{OH,ads}}{\rightleftharpoons}} OH* + H^+ + e^- \quad (r6)$$

$$CO_L + OH* \xrightarrow{k_I} CO_2 + H^+ + e^- + 2* \quad (r7)$$

$$FA_S^- + * \xrightarrow{k_D} CO_2 + H^+ + 2e^- + * \quad (r8)$$

The externally applied potential (E_{app}) is defined with respect to a reference electrode, such that any uncompensated resistance (R_U) results in a difference between E_{app} and the true surface potential (ϕ). Thus, a sinusoidal input and the resulting simulated total current density (j_{TOT}) were modeled using the following expressions:

$$E_{app} = A \sin(2\pi f^* t) + E_{DC} \quad (1)$$

$$j_{TOT} = \frac{E_{app} - \phi}{SA^* R_U} \quad (2)$$

where A is the amplitude and f is the frequency, respectively, of the applied potential-modulation, E_{DC} is the potential at which the modulation is centered, and SA is the electrode surface area. To best match experimental conditions, we employed the values SA = 0.4 cm^2 and R_U = 40 Ω.

The rate equations (with the exception of purely thermal mass transfer and surface diffusion coefficients) are based on the Butler−Volmer approximation of rate constants in the form

$$k_i = k_i^0 \exp\left[\frac{\beta_i F}{RT}(\phi - \phi_i)\right] \quad (3)$$

where ϕ_i is fit to experimental data,[1] k_i^0 is set to unity (mathematically arbitrary with ϕ_i fitted), β_i is assumed[33] to be 0.5 (−0.5 for reduction steps), unless otherwise indicated, F = 96 485.33 C/mol, R = 8.314 J/(mol K), and T = 298.15 K. Therefore, the rate equations for all reaction steps can be represented by the following expressions:

$$\nu_m = k_m C_{FA_{Bulk}} \quad (v1)$$

$$\nu_{FA,ads} = k_{FA,ads} C_{FA_S} \theta_v^2 \quad (v2f)$$

$$\nu_{FA,des} = k_{FA,des} \theta_{FA_B} \quad (v2r)$$

$$\nu_{FA,diff} = k_{FA,diff} \theta_{FA_B} \theta_v^2 \quad (v3)$$

$$\nu_F = k_F \theta_{FA_L} \theta_v \quad (v4)$$

$$\nu_P = k_P \theta_{FA_L} \theta_v^2 \quad (v5)$$

$$\nu_{OH,ads} = k_{OH,ads} C_{H_2O} \theta_v \quad (v6f)$$

$$\nu_{OH,des} = k_{OH,des} \theta_{OH} \quad (v6r)$$

$$\nu_I = k_I \theta_{CO_L} \theta_{OH} \quad (v7)$$

$$\nu_D = k_D C_{FA_S^-} \theta_v \quad (v8)$$

Above, vacant sites and formate/formic acid equilibrium are defined by

$$\theta_v = 1 - 1.516\theta_{CO_L} - \theta_{FA_L} - 2\theta_{FA_B} - \theta_{OH} \quad (4)$$

$$C_{FA_S^-} = K_A C_{FA_S} \quad (5)$$

where the coverage of linear-bound CO_L* is corrected to account for the fast equilibrium of the harder-to-oxidize bridge-bound CO_B*, estimated by the relation $\theta_{CO_B} \approx 0.258\ \theta_{CO_L}$.[1] The concentration of deprotonated formic acid (formate) is represented by $C_{FA_S^-}$ and is determined as a function of the solution pH by the equilibrium constant K_A.

The resulting system of ODEs from population balances and coupled process variables is given as

$$\frac{d\theta_{FA_B}}{dt} = \nu_{FA,ads} - \nu_{FA,des} - \nu_{FA,diff} \quad (6)$$

$$\frac{d\theta_{FA_L}}{dt} = \nu_{FA,diff} - \nu_P - \nu_F \quad (7)$$

$$\frac{d\theta_{CO_L}}{dt} = \nu_P - \nu_I \quad (8)$$

https://dx.doi.org/10.1021/acs.iecr.0c04414
Ind. Eng. Chem. Res. 2020, 59, 19999−20010

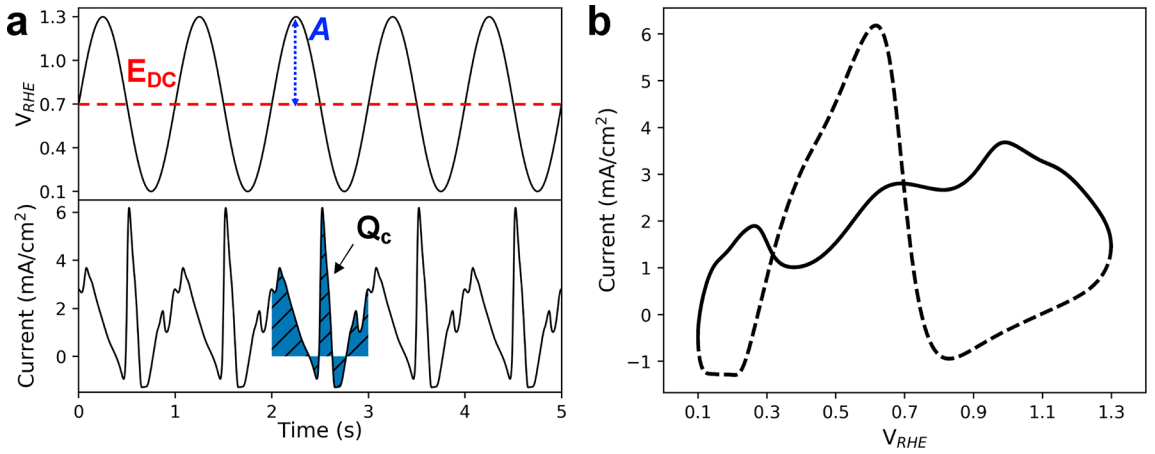

Figure 1. Rotating disk voltammetry of the current response from a sine waveform potential modulation (a) versus time and (b) versus voltage during the electro-oxidation of 0.1 M formic acid in 0.1 M $HClO_4$ at a Pt disk electrode. Cycle-time averaged current was determined by integrating the charge passed per cycle. E_{DC} = 0.7 V_{RHE}, A = 0.6 V, f = 1 Hz. The forward (anodic) sweep in panel (b) is the solid line and the reverse (cathodic) sweep is the dotted line. Rotation rate = 2500 rpm.

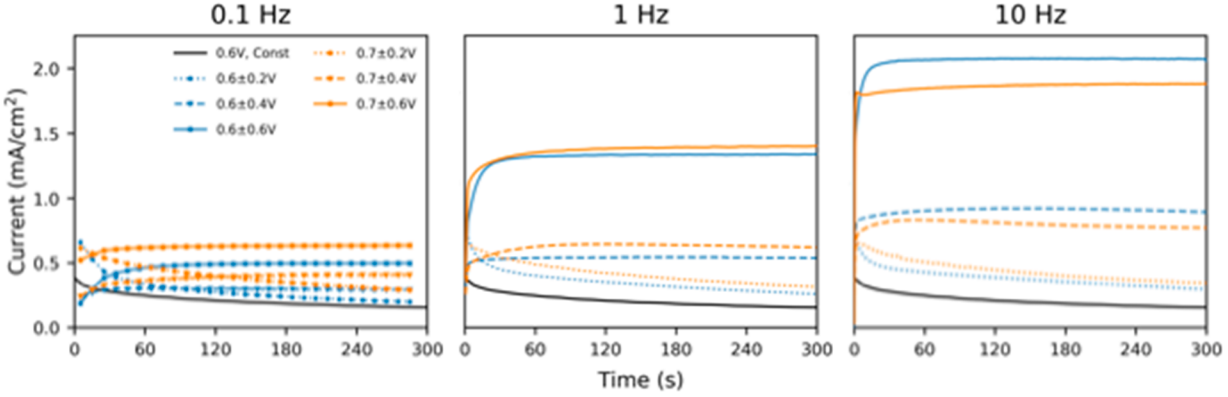

Figure 2. Rotating disk chronoamperometry of polycrystalline Pt RDE tip with 0.1 M formic acid in 0.1 M $HClO_4$ for 300 s at f = 0.1, 1, and 10 Hz at various E_{DC} and A. Rotation rate = 2500 rpm. Discrete data points for the 0.1 Hz experiment are marked.

$$\frac{d\theta_{OH}}{dt} = \nu_{OH,ads} - \nu_{OH,des} - \nu_I \quad (9)$$

$$\frac{dC_{FA_S}}{dt} = \frac{2k_m}{\delta^2}(C_{FA_{Bulk}} - C_{FA_S}) - \frac{2S_{TOT}}{\delta}(\nu_{FA,ads} + \nu_D) \quad (10)$$

$$\frac{d\phi}{dt} = \frac{1}{C_{DL}}(j_{TOT} - j_f) \quad (11)$$

The resulting Faradaic current density can then be represented by

$$j_f = FS_{TOT}(\nu_{FA,ads} + \nu_F + \nu_{OH,ads} + \nu_I + 2\nu_D - \nu_P - \nu_{OH,des}) \quad (12)$$

RESULTS AND DISCUSSION

Voltammetry Studies. As a first step to understanding where such an oscillatory enhancement regime may exist, rotating disk chronoamperometry experiments were performed on a Pt disk applying a sinusoidal potential waveform at DC offset potentials ranging from 0.4 V to 0.9 V (E_{DC}), frequencies ranging from 0.1 Hz to 10 Hz, and amplitudes ranging from 0 V to 0.6 V. Experiments were limited to this waveform frequency range because of a maximum data point readout acquisition frequency of 4 kHz in the digital system (ensuring minimum 400 points per cycle). Prior to each experiment, the potential was held at 1.0 V for 30 s to limit the buildup of CO*, which could skew initial oxidation currents. A stable example of the subsequent current response at 0.7 ± 0.6 V and f = 1 Hz is shown in Figure 1. The current versus potential plot (Figure 1a) shows a stable response to the sinusoidal waveform and is analogous to a cyclic voltammetry experiment at 2.4 V/s over a potential range of 0.1−1.3 V. Oxidation peaks appear on both the forward and reverse sweeps: the higher peak in the forward sweep is attributable to a combination of the direct, indirect, and formate pathways, while the secondary peak in the reverse sweep is thought to be primarily attributable to the direct pathway.[2]

In order to compare cases with potential modulation to the fixed-potential controls, the average Faradaic current was determined by integrating the total charge passed per cycle (Q_c) and normalizing by the period of the oscillation. This procedure effectively cancels out current resulting from capacitive and pseudocapacitive processes such as the charging/discharging of the electrochemical double layer, underpotential deposition/stripping of H*, and oxidation/reduction of the Pt surface during the potential modulation. Regions with possible parasitic faradaic currents that are due to hydrogen and oxygen evolution reactions (HER and OER, respectively) were also assessed in control experiments. First, all

https://dx.doi.org/10.1021/acs.iecr.0c04414
Ind. Eng. Chem. Res. 2020, 59, 19999−20010

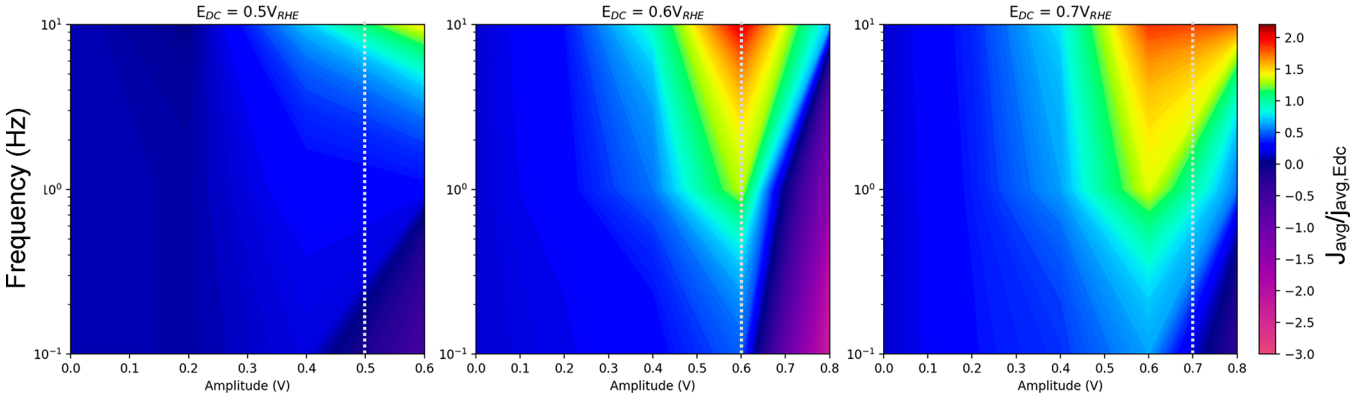

Figure 3. Heat maps showing the averaged current density over the final 60 s of rotating disk chronoamperometry experiments and normalized by the current density during the potentiostatic experiments at each E_{DC}. Data points shown correspond to increments of A = 0.2 V and f = 0.1, 1, and 10 Hz. Vertical lines correspond to $A = E_{DC}$(waveform reaching 0 V_{RHE}). HER onset begins slightly positive of 0 V and begins to detract from the formic acid current. Suppression of HER is seen at 10 Hz for all $A < E_{DC}$ (blank electrolyte runs in Figure S2).

waveform conditions presented in the RDE cell were examined in blank electrolyte (no formic acid). These show the region of HER onset near 0 V, but rule out the contribution of additive oxidation currents from the OER (see Figure S2 in the Supporting Information). For conditions that do not create H_2, linearity of CO_2 production rate versus net current (as well as lack of O_2) were confirmed using gas chromatography in a gas-tight batch cell under conditions comparable to those used in the RDE experiments (see Figure S3 in the Supporting Information). H_2 was not assayed, but it was always found that net currents decrease when waveforms reach 0 V, and thus these conditions are not ideal for enhancing selective oxidation. A comparison of the effect of several E_{DC}, amplitudes, and frequencies on the net current over 300 s is shown in Figure 2. The increase in Faradaic current density was observed to be most sensitive to increases in the frequency of the applied potential waveform. Increasing the amplitude was also found to increase the resulting current, but only until the lower potential bound (E_L) fell at or below 0 V, where the onset of the HER began to skew current in the negative direction. The decay of the current density over time was most influenced by the higher potential bound (E_H), with resistance to deactivation onsetting at an E_H value near 1.0 V, as seen by a reversal in trend to rising initial activity (as opposed to decay) and resulting stable currents at all frequencies.

To better understand the trends across modulation conditions and to better contrast with the proceeding modeling work, the relative increase in current density was estimated by normalizing the average current density during the final 60 s of the experiment against the current density under potentiostatic conditions obtained in the same manner at each E_{DC}. This is summarized in the form of heat maps, and select comparisons are shown in Figure 3 (the full range of E_{DC} and controls run with no formic acid present can be found in Figures S1 and S2, respectively, in the Supporting Information). Each heat map shows a similar trend with the peak increase in current density found as the amplitude approaches the value of E_{DC} at f = 10 Hz. While the normalized currents might be thought of as an "enhancement factor", this must be qualified by two observations. First, the potentiostatic current is still actively decaying at 300 s; the observed current under oscillatory conditions is considerably more stable, and thus the enhancement increases over time. Second, at amplitudes approaching, or greater than, E_{DC}, the net oxidation current decreases as the current density decreases, resulting from the HER becoming increasingly prominent. This effect is most prominent at low frequency, where HER is so dominant that the net current is negative. Per Figure S2, higher frequency appears to suppress HER, so its contribution likely also decreases during the conditions yielding the highest formic acid oxidation rates.

To confirm that potential modulation reduces deactivation compared to the potentiostatic base case, a potential-modulation experiment was repeated at E_{DC} = 0.7 V, f = 0.1–10 Hz, A = 0–0.6 V over a longer time period of 1 h. Results for A = 0, 0.4, and 0.6 are summarized in Figure 4. As expected, the

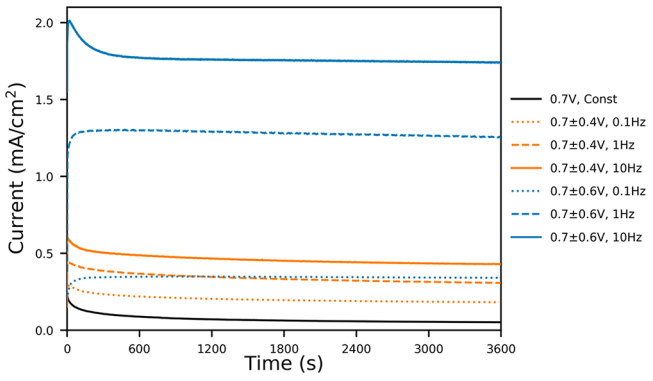

Figure 4. Rotating disk chronoamperometry of polycrystalline Pt RDE tip with 0.1 M formic acid in 0.1 M $HClO_4$ for 3600 s at E_{DC} = 0.7 V, f = 0.1–10 Hz, and A = 0–0.6 V. Rotation rate = 2500 rpm.

potentiostatic current continues to decay over the course of the experiment, falling by an additional ~60% between 300 s and the 1-h mark. Oscillating at A = 0.2 (Figure S4 in the Supporting Information) resulted in no difference, compared to the potentiostatic case at 0.7 V. In contrast, the best oscillatory case for stability among the modulation parameters tested was found at 0.7 ± 0.6 V at f = 10 Hz. This condition resulted in an ~31-fold increase, compared to potentiostatic operation at 0.7 V, and an ~27-fold increase in current density, compared to the best potentiostatic case at 0.6 V (see Figure S4). In addition, while there was still some deactivation in the best potential-modulated case, the current density only decreased by ~7% from 300 s to the 1-h mark, suggesting that there is room for optimization, both toward rate and stability.

https://dx.doi.org/10.1021/acs.iecr.0c04414
Ind. Eng. Chem. Res. 2020, 59, 19999–20010

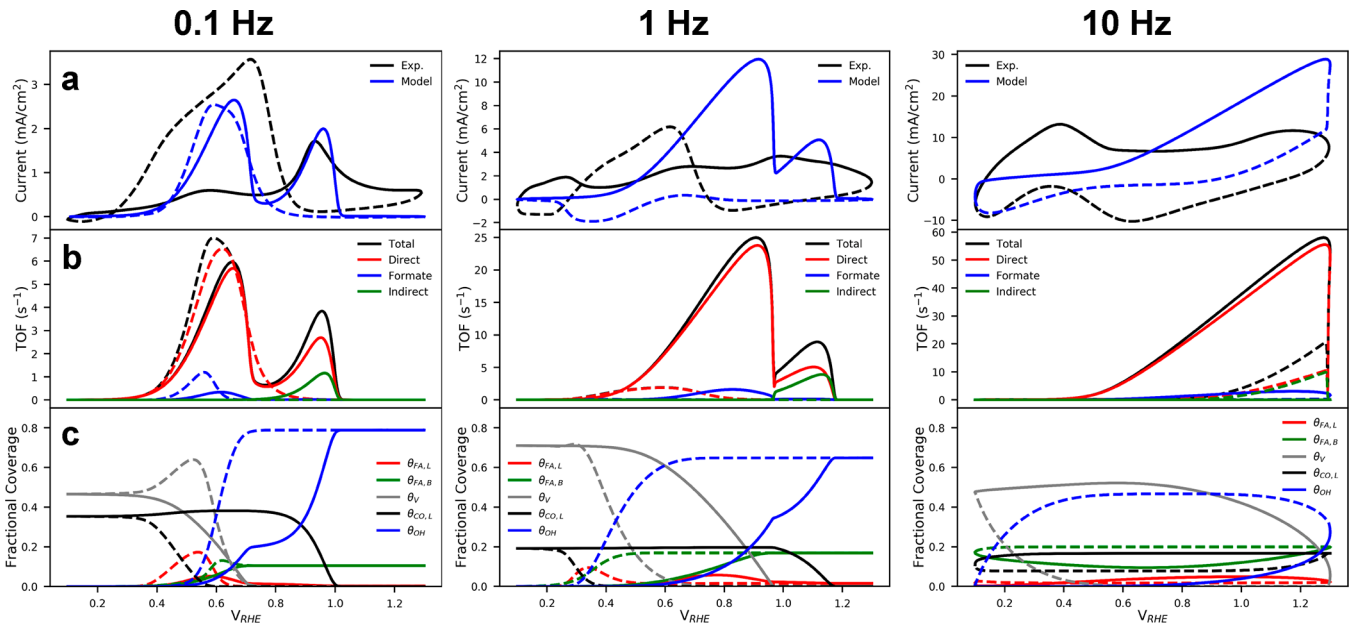

Figure 5. Simulated potential oscillation based on the microkinetic model adapted from Calderón-Cárdenas et al. showing (a) a comparison of experimentally observed (black) versus simulated current density (blue), (b) simulated TOFs for the formation of CO_2 via each pathway (legend: black, total; red, direct; blue, formate; and green, indirect), and (c) fractional surface coverages of all intermediates (legend: red, FA_L^*; green, FA_B^*; gray, free sites; black, CO_L^*; and blue, OH*; CO_B^* (not shown) is governed by $\theta_{CO,B} = 0.258\ \theta_{CO,L}$). The forward (anodic) sweep is the solid line and the reverse (cathodic) sweep is the dotted line. Parameters: f = 0.1, 1, and 10 Hz, E_{DC} = 0.7 V, and A = 0.6 V.

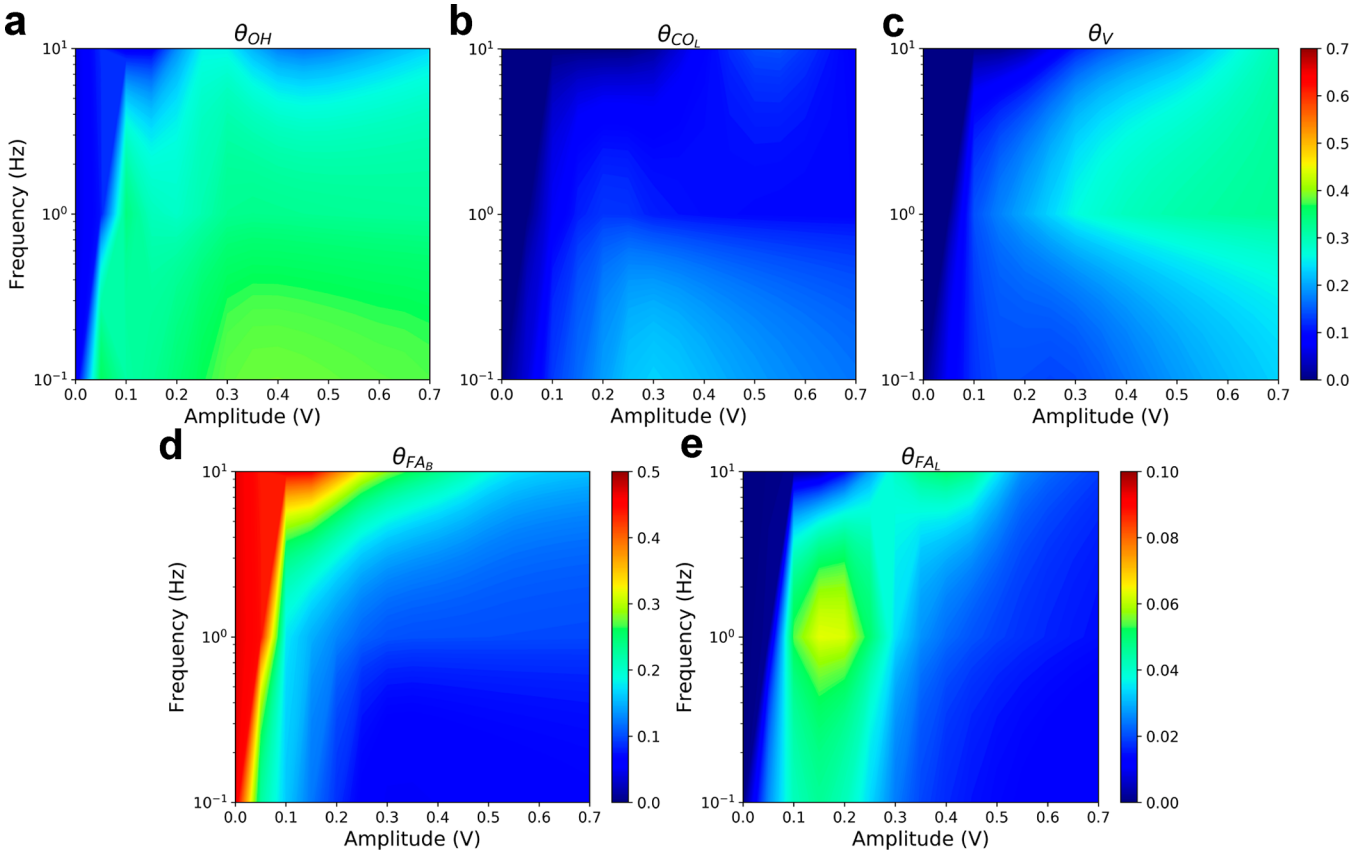

Figure 6. Simulated heat maps at E_{DC} = 0.7 V showing the cycle-average surface coverage of (a) OH*, (b) CO_L^*, (c) free sites, (d) FA_B^*, and (e) FA_L^*. The same scale bar applies for panels (a)−(c). Data points shown correspond to increments of A = 0.05 V ($\pm E_{DC}$) and f = 0.1, 0.25, 0.5, 0.75, 1, 2.5, 5, 7.5, and 10 Hz, resulting in a 15 × 9 grid.

Microkinetic Modeling. To further understand the mechanism behind the ∼30-fold increase in formic acid oxidation activity and increased resistance to deactivation, a microkinetic model (MKM) was adapted from Calderón-

https://dx.doi.org/10.1021/acs.iecr.0c04414
Ind. Eng. Chem. Res. 2020, 59, 19999−20010

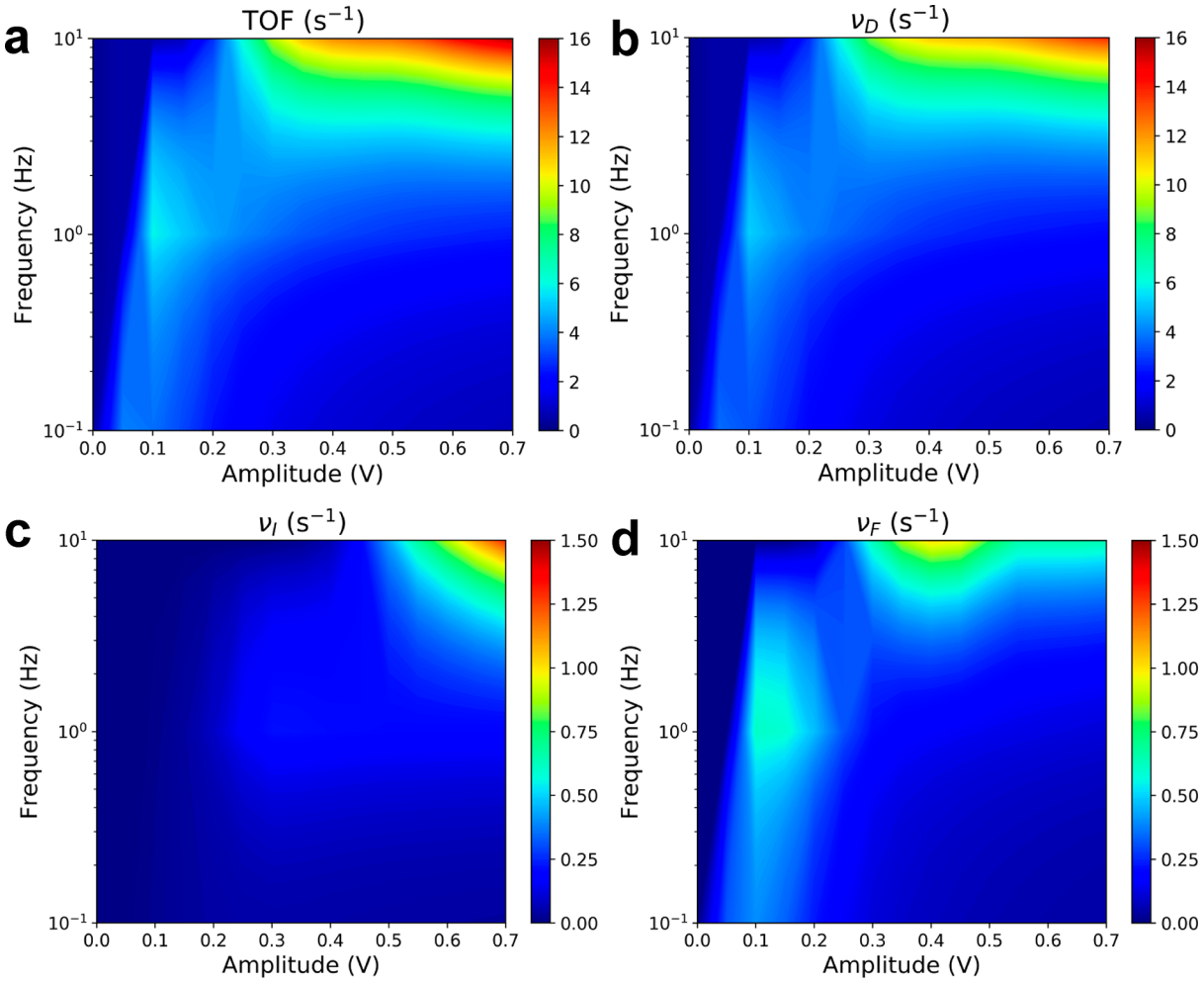

Figure 7. Simulated heat maps at E_{DC} = 0.7 V showing TOF for the (a) combined total, (b) direct, (c) indirect, and (d) formate pathways over a range of A and f. Data points shown correspond to increments of A = 0.05 V ($\pm E_{DC}$) and f = 0.1, 0.25, 0.5, 0.75, 1, 2.5, 5, 7.5, and 10 Hz, resulting in a 15 × 9 grid.

Cárdenas et al.[1] and modified to include the mass transport effects of our RDE experiments with a diffusion layer (summarized in Scheme 3). The output from a simulated oscillation experiment at 0.7 ± 0.6 V at f = 1 Hz is shown in Figure 5. Because of the fact that the MKM does not explicitly account for nonreactive, pseudocapacitive processes such as H underpotential deposition/stripping and the oxidation/reduction of the Pt surface (past OH* formation), the model is only able to provide a qualitative understanding of the underlying processes that likely occur during a stable oscillation experiment. Deviations caused by these pseudocapacitive processes reflect an increasing ratio of their respective contribution in parallel to the reaction and are most pronounced at higher frequency—i.e., the reaction is occurring with fewer turnovers per cycle on top of these backgrounds, despite the higher rates netted by more cycles per unit time. Nonetheless, the simulated current density at 0.1 Hz shows consistency with experimental data (Figure 5a), and some qualitative features are still seen at 1 Hz before the pseudocapacitances (which contribute no net current) begin to dominate the measurements at 10 Hz.

The MKM reveals the respective TOF for each oxidation pathway and how it contributes to the simulated current density (Figure 5b); the onset potential of each pathway was consistent with experimental results at f = 0.1 Hz, with the direct and formate paths operable near the onset of measurable current and the indirect path lighting off much later, ~0.8 V.[2] In addition, the model enables an analysis of the fractional surface coverage for each of the reaction intermediates (Figure 5c). Beginning at ~0.1 V and following along the anodic sweep (solid line), just over a third of the surface is covered in CO_L* (with a smaller additional contribution from equilibrated CO^*_B, not shown). The total CO* population is much lower than the potentiostatic steady state (see Figure 6b), while almost half of the surface is vacant and available for the potential-dependent adsorption of either FA^*_B (bridge-bound formate) or OH*. As potential rises and FA^*_B builds up on the surface and (thermally) reorients to form FA^*_L, the formate pathway becomes operative as a minor route (onsetting at ~0.5 V), with the kinetically favorable direct pathway still dominating between 0.4 and 1.0 V. At ~0.8 V, the combination of increasing amounts of OH* and large overpotential results in the indirect pathway lighting off, clearing the surface of the strongly bound CO* typically associated with deactivation under potentiostatic conditions. At even higher overpotential (>1.1 V), the surface is effectively blocked by a combination of OH* and FA^*_B, and the reaction rate decreases dramatically. This trend remains along the cathodic sweep (dotted lines) until ~0.6 V, where OH* begins to undergo reductive desorption. As more vacant sites become available, the strongly bound FA^*_B again undergoes the non-Faradaic reaction to FA^*_L, which, in turn, is increasingly reduced to CO*. This

https://dx.doi.org/10.1021/acs.iecr.0c04414
Ind. Eng. Chem. Res. 2020, 59, 19999−20010

finding suggests that the increase in activity observed during potential oscillations cannot be attributed solely to the notion that periodically raising the potential "clears" the surface of strongly bound intermediates, but that the clearing facilitates the formation of new, oxidizable FA_L^* and CO* species, eventually resulting in an increased flux through both the indirect and formate pathways. Oxidation via the formate pathway is also increased, albeit to a significantly lesser extent.

The cycle-averaged attributes output by the MKM are summarized utilizing heat maps, with fractional surface coverages shown in Figure 6 and TOFs via each pathway shown in Figure 7 for E_{DC} = 0.7 V. (Additional heat maps for each MKM output at E_{DC} = 0.4−0.7 V can be found in Figures S5−S18 in the Supporting Information). The surface coverages of the primary intermediates (CO* and OH*; see Figures 6a and 6b) are generally found to decrease as the f and A values increase, but the resulting increase in vacant sites, relative to potentiostatic conditions (Figure 6c), does not completely align with the activity "hotspot" region experimentally observed at high A values (approaching E_{DC} at high, constant f). While the highest activity is reached at $E_{DC} = A$, activity begins rising at lower values of A, where the vacancy coverage is actually still quite low. Examining the surface coverages of formate species (Figures 6d and 6e) reveals that the relative abundance, particularly of FA_L^*, actually increases in the region of high f and intermediate A values, suggesting that increased formate adsorption and flux through the formate path are present at $A \approx$ 0.3−0.5 V in the "hotspot". This finding is consistent across all simulated E_{DC} values (Figures S10−S14 in the Supporting Information) and provides evidence that the increased oxidation rate during oscillation is not solely the result of maintaining more reaction sites for the direct pathway to proceed.

Evaluating how the TOF through each oxidation pathway changes over this range of A and f provides more insight into how the net reaction rate is increased under oscillation conditions (see Figure 7). The simulated total TOF (Figure 7a) aligns well with the previously presented experimental TOF versus A and f (Figure 3), further suggesting that the model captures a majority of the important processes involved in the mechanism. It is clear from the model that, while the direct pathway is still the primary route for formic acid oxidation (Figure 7b), flux through both the indirect (Figure 7c) and formate (Figure 7d) pathways increases at values of A and f, where potential modulation results in the highest observed reaction rates. Together with the findings from the surface coverage simulations at other E_{DC} values, this suggests that the increased oxidation rate can be attributed to the acceleration of all three pathways (~20% of the oxidation proceeding through the formate and indirect pathways at 0.7 ± 0.6 V, f = 10 Hz). The resulting catalytic cycle is summarized in Scheme 4. Beginning at low potentials (<0.4 V), the Pt surface is covered primarily in CO*, accompanied by significantly less FA_L^*, as well as a portion of the surface free of adsorbates. As the potential rises, solution-phase formic acid is able to undergo direct oxidation while a portion is oxidatively absorbed alongside OH*, and while FA_L^* is oxidized via the formate pathway. At potentials >0.9 V, the CO* is removed via the indirect pathway and the resulting surface is effectively poisoned by both OH* and FA_B^*, thus shutting down all pathways of oxidation. As the potential is then reversed and lowered to more reducing potentials, the OH* is reductively desorbed, thus freeing surface sites for FA_B^* to reorient to FA_L^* while allowing the direct pathway to proceed again. As the potential returns below ~0.4 V, a majority of this FA_L^* undergoes

Scheme 4. Proposed Catalytic Cycle for the Oscillatory Electro-oxidation of Formic Acid on a Pt Electrode Based on Microkinetic Model Simulations and Experimental Observations[a]

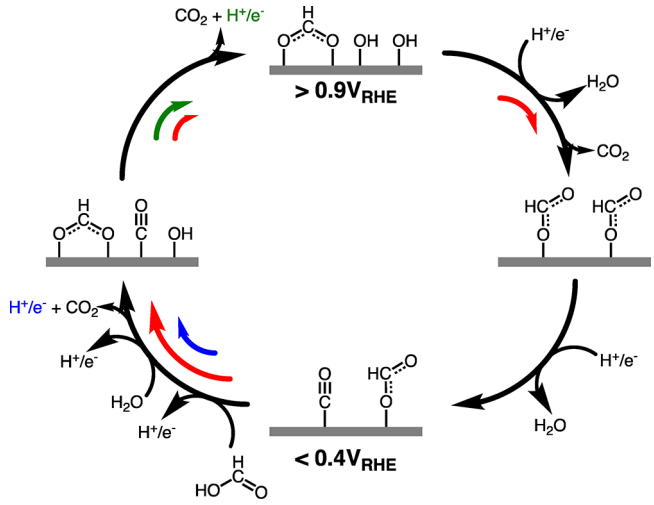

[a]The color of each arrow corresponds to the major pathway(s) at each step (red, direct: blue, formate: green, indirect) and the magnitudes represent the relative flux through the respective pathway.

a net reduction to form CO* and the cycle begins again. These low-potential processes thus actually facilitate the formation of intermediates for both the formate and indirect pathways, resulting in an accelerated rate for both upon increasing the potential again. While enough of the surface is kept free of adsorbates to allow the direct pathway to continue to proceed and the total activity to be maintained over time, this finding suggests that the observed increase in formic acid oxidation cannot solely be attributed to maintaining a "clear" reactive surface; all of the pathways collectively proceed at higher rates than observed under potentiostatic conditions.

CONCLUSIONS

This work explored applying methods of potential-modulated stimulation of electrocatalytic activity (PSEA) to the electro-oxidation of formic acid via a sinusoidal potential modulation. Rotating disk chronoamperometry experiments revealed that applying a wave with E_{DC} > 0.5 V and an A > 0.5 V resulted in a current density that was higher than that observed under optimal potentiostatic conditions; furthermore, the PSEA approach improved resistance to deactivation as a result of the buildup of spectator adsorbates. The largest increase in activity was observed during an hour-long experiment at 0.7 ± 0.6 V with f = 10 Hz and was found to be ~30-fold higher than the potentiostatic experiment at 0.7 V, holding all other factors constant. The resistance to deactivation during modulation was characterized by a decrease of only 7% between 5 and 60 min of continuous operation, compared to a 60% decrease under the most active potentiostatic conditions (0.6 V). A microkinetic model was utilized as a qualitative means of understanding how the underlying reaction pathways contribute to the increase in activity. While a majority of the increased activity is due to the periodic clearing of strongly bound CO* from the surface, the model suggests that the potential oscillations actually increase the rates of both the indirect and formate pathways by facilitating the initial formation of FA_L^*, and subsequently CO*, during the cathodic sweep. Based on these findings, we

https://dx.doi.org/10.1021/acs.iecr.0c04414
Ind. Eng. Chem. Res. 2020, 59, 19999−20010

suggest that high fidelity kinetic modeling, combined with advanced optimization techniques, could be used to customize waveforms to achieve even higher activity, stability, and selectivity in formic acid oxidation and many other reactions. PSEA methods thus show promise as a means of accelerating electrocatalytic reactions, as well as for aiding in discernment of mechanistic aspects of these reactions.

■ ASSOCIATED CONTENT

Supporting Information

The Supporting Information is available free of charge at https://pubs.acs.org/doi/10.1021/acs.iecr.0c04414.

Heat maps showing cycle-averaged currents during the final 60 s of a 300 s experiment with 0.1 M formic acid (Figure S1) and without formic acid (Figure S2); GC confirmation of linearity between CO_2 and charged passes (Figure S3); complete data set for chronoamperometry experiments run for 3600 s (Figure S4); and all cycle-averaged attributes found in model simulation results (Figures S5−S18) (PDF)

■ AUTHOR INFORMATION

Corresponding Author

Adam Holewinski − *Department of Chemical and Biological Engineering and Renewable and Sustainable Energy Institute, University of Colorado, Boulder, Colorado 80303, United States;* orcid.org/0000-0001-8307-5881; Email: adam.holewinski@colorado.edu

Authors

Alex M. Román − *Department of Chemical and Biological Engineering and Renewable and Sustainable Energy Institute, University of Colorado, Boulder, Colorado 80303, United States;* orcid.org/0000-0003-0221-4355

Taylor D. Spivey − *Department of Chemical and Biological Engineering and Renewable and Sustainable Energy Institute, University of Colorado, Boulder, Colorado 80303, United States;* orcid.org/0000-0001-6915-6220

J. Will Medlin − *Department of Chemical and Biological Engineering and Renewable and Sustainable Energy Institute, University of Colorado, Boulder, Colorado 80303, United States;* orcid.org/0000-0003-2404-2443

Complete contact information is available at: https://pubs.acs.org/10.1021/acs.iecr.0c04414

Notes

The authors declare no competing financial interest.

Biographies

Alex M. Román earned his Ph.D. in Chemical Engineering from the University of Colorado−Boulder in 2020, which was funded by an NSF Graduate Research Fellowship and under the joint supervision of J. Will Medlin and Adam Holewinski. He received his Bachelor of Chemical Engineering from Auburn University in 2014. He is currently working as a Senior Chemical Engineer at Pioneer Astronautics in Lakewood, CO.

Taylor D. Spivey is a Ph.D. student in chemical engineering advised by Adam Holewinski at the University of Colorado−Boulder. He received his Bachelor of Chemical Engineering from the University of Tennessee in 2018. His research interests include heterogeneous catalysis, electrochemistry, and the application to X-ray spectroscopic methods to understand these processes. He was recently awarded a DOC SCGSR fellowship to pursue developing in situ X-ray techniques.

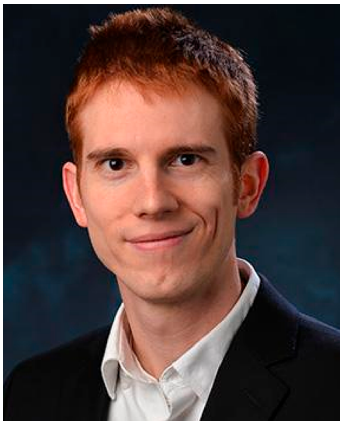

Adam Holewinski is an Assistant Professor of Chemical and Biological Engineering at the University of Colorado−Boulder and a Fellow of the CU-NREL Renewable and Sustainable Energy Institute. He received

https://dx.doi.org/10.1021/acs.iecr.0c04414
Ind. Eng. Chem. Res. 2020, 59, 19999−20010

B.S.E. and Ph.D. degrees from the University of Michigan, followed by Postdoctoral work at the Georgia Institute of Technology before joining University of Colorado−Boulder in 2015. He has received several recognitions, including an NSF CAREER award. His research interests lie in heterogeneous catalysis and electrochemistry for sustainable production of energy and chemicals, with emphasis on characterization through kinetics, spectroscopy, and modeling.

■ ACKNOWLEDGMENTS

A.M.R. acknowledges support from the NSF Graduate Research Fellowship (No. 1144083). T.D.S. acknowledges support from the Graduate Assistantship In Areas of National Need funded by the U.S. Department of Education. The authors acknowledge support from the National Science Foundation (No. CHE 1665176). This work utilized the RMACC Summit supercomputer, which is supported by NSF Award Nos. ACI-1532235 and ACI-1532236, the University of Colorado−Boulder, and Colorado State University. The Summit supercomputer is a joint effort of the University of Colorado−Boulder and Colorado State University. The authors would also like to thank Dr. Zack Barton for helpful discussion and insight.

■ REFERENCES

(1) Calderón-Cárdenas, A.; Hartl, F. W.; Gallas, J. A. C.; Varela, H. Modeling the triple-path electro-oxidation of formic acid on platinum: Cyclic voltammetry and oscillations. *Catal. Today* **2019**, 1−9.

(2) Cuesta, A.; Cabello, G.; Osawa, M.; Gutiérrez, C. Mechanism of the Electrocatalytic Oxidation of Formic Acid on Metals. *ACS Catal.* **2012**, *2*, 728−738.

(3) Perales-Rondón, J. V.; Brimaud, S.; Solla-Gullón, J.; Herrero, E.; Behm, R. J.; Feliu, J. M. Further Insights into the Formic Acid Oxidation Mechanism on Platinum: pH and Anion Adsorption Effects. *Electrochim. Acta* **2015**, *180*, 479−485.

(4) Joo, J.; Uchida, T.; Cuesta, A.; Koper, M. T. M.; Osawa, M. Importance of acid-base equilibrium in electrocatalytic oxidation of formic acid on platinum. *J. Am. Chem. Soc.* **2013**, *135*, 9991−9994.

(5) Okamoto, H.; Numata, Y.; Gojuki, T.; Mukouyama, Y. Different behavior of adsorbed bridge-bonded formate from that of current in the oxidation of formic acid on platinum. *Electrochim. Acta* **2014**, *116*, 263−270.

(6) Mei, D.; He, Z.-D.; Jiang, D. C.; Cai, J.; Chen, Y.-X. Modeling of Potential Oscillation during Galvanostatic Electrooxidation of Formic Acid at Platinum Electrode. *J. Phys. Chem. C* **2014**, *118*, 6335−6343.

(7) Strasser, P.; Eiswirth, M.; Ertl, G. Oscillatory instabilities during formic acid oxidation on Pt(100), Pt(110) and Pt(111) under potentiostatic control. II. Model calculations. *J. Chem. Phys.* **1997**, *107*, 991−1003.

(8) Koper, M. T. M.; Schmidt, T. J.; Markovic, N. M.; Ross, P. N. Potential Oscillations and S-Shaped Polarization Curve in the Continuous Electro-oxidation of CO on Platinum Single-crystal Electrodes. *J. Phys. Chem. B* **2001**, *105*, 8381−8386.

(9) Strmcnik, D. S.; Rebec, P.; Gaberscek, M.; Tripkovic, D.; Stamenkovic, V.; Lucas, C.; Markovic, N. M. Relationship between the Surface Coverage of Spectator Species and the Rate of Electrocatalytic Reactions. *J. Phys. Chem. C* **2007**, *111*, 18672−18678.

(10) Engstfeld, A. K.; Brimaud, S.; Behm, R. J. Potential-Induced Surface Restructuring-The Need for Structural Characterization in Electrocatalysis Research. *Angew. Chem., Int. Ed.* **2014**, *53*, 12936−12940.

(11) Wang, S.-R.; Fedkiw, P. S. Pulsed-Potential Oxidation of Methanol. *J. Electrochem. Soc.* **1992**, *139*, 2519−2524.

(12) Ardagh, M. A.; Abdelrahman, O. A.; Dauenhauer, P. J. Principles of Dynamic Heterogeneous Catalysis: Surface Resonance and Turnover Frequency Response. *ACS Catal.* **2019**, *9*, 6929−6937.

(13) Gopeesingh, J.; Ardagh, M. A.; Shetty, M.; Burke, S.; Dauenhauer, P. J.; Abdelrahman, O. A. Resonance-Promoted Formic Acid Oxidation via Dynamic Electrocatalytic Modulation. *ACS Catal.* **2020**, *10* (17), 9932−9942.

(14) Baz, A.; Holewinski, A. Understanding the interplay of bifunctional and electronic effects: Microkinetic modeling of the CO electro-oxidation reaction. *J. Catal.* **2020**, *384*, 1−13.

(15) Grozovski, V.; Climent, V.; Herrero, E.; Feliu, J. M. Intrinsic Activity and Poisoning Rate for HCOOH Oxidation at Pt(100) and Vicinal Surfaces Containing Monoatomic (111) Steps. *ChemPhysChem* **2009**, *10*, 1922−1926.

(16) Grozovski, V.; Climent, V.; Herrero, E.; Feliu, J. M. Intrinsic activity and poisoning rate for HCOOH oxidation on platinum stepped surfaces. *Phys. Chem. Chem. Phys.* **2010**, *12*, 8822−10.

(17) Grozovski, V.; Solla-Gullón, J.; Climent, V.; Herrero, E.; Feliu, J. M. Formic Acid Oxidation on Shape-Controlled Pt Nanoparticles Studied by Pulsed Voltammetry. *J. Phys. Chem. C* **2010**, *114*, 13802−13812.

(18) Clavilier, J. Pulsed linear sweep voltammetry with pulses of constant level in a potential scale, a polarization demanding condition in the study of platinum single crystal electrodes. *J. Electroanal. Chem. Interfacial Electrochem.* **1987**, *236*, 87−94.

(19) Fedkiw, P. S.; Scott, W. D. Selectivity Changes in Electrochemical Reaction Sequences by Modulated Potential Control. *J. Electrochem. Soc.* **1984**, *131*, 1304−1315.

(20) Fedkiw, P. S.; Traynelis, C. L.; Wang, S.-R. Pulsed-Potential Oxidation of Methanol. *J. Electrochem. Soc.* **1988**, *135*, 2459−2465.

(21) Wang, S.-R.; Fedkiw, P. S. Pulsed-Potential Oxidation of Methanol. *J. Electrochem. Soc.* **1992**, *139*, 3151−3158.

(22) Blanco, D. E.; Lee, B.; Modestino, M. A. Optimizing organic electrosynthesis through controlled voltage dosing and artificial intelligence. *Proc. Natl. Acad. Sci. U. S. A.* **2019**, *116*, 17683−17689.

(23) Kokoh, K. B.; Belgsir, E. T. Electrosynthesis of furan-2,5-dicarbaldehyde by programmed potential electrolysis. *Tetrahedron Lett.* **2002**, *43*, 229−231.

(24) Glenn, B. C.; Saunders, J. H. Optimal Performance from Electrochemical Devices Using Control Theory at the Surface Coverage Level. *J. Electrochem. Soc.* **2011**, *159*, B165−B172.

(25) Carrette, L. P. L.; Friedrich, K. A.; Huber, M.; Stimming, U. Improvement of CO tolerance of proton exchange membrane (PEM) fuel cells by a pulsing technique. *Phys. Chem. Chem. Phys.* **2001**, *3*, 320−324.

(26) Bakshi, R.; Fedkiw, P. S. Optimal Time-Varying Cell-Voltage Control of a Parallel-Plate Reactor. *J. Appl. Electrochem.* **1994**, *24*, 1116−1123.

(27) Adzic, R. R.; Popov, K. I.; Pamić, M. A. Acceleration of electrocatalytic reactions by pulsation of potential: Oxidation of formic acid on Pt and Pt/Pbads electrodes. *Electrochim. Acta* **1978**, *23*, 1191−1196.

(28) Okamoto, H.; Tanaka, N.; Naito, M. Modelling temporal kinetic oscillations for electrochemical oxidation of formic acid on Pt. *Chem. Phys. Lett.* **1996**, *248*, 289−295.

(29) Zhu, X.; Huang, J. Modeling Electrocatalytic Oxidation of Formic Acid at Platinum. *J. Electrochem. Soc.* **2020**, *167*, 013515.

(30) Hsu, S.-H.; Stamatis, S. D.; Caruthers, J. M.; Delgass, W. N.; Venkatasubramanian, V.; Blau, G. E.; Lasinski, M.; Orcun, S. Bayesian Framework for Building Kinetic Models of Catalytic Systems. *Ind. Eng. Chem. Res.* **2009**, *48*, 4768−4790.

(31) Virtanen, P.; Gommers, R.; Oliphant, T. E.; Haberland, M.; Reddy, T.; Cournapeau, D.; Burovski, E.; Peterson, P.; Weckesser, W.; Bright, J.; van der Walt, S. J.; Brett, M.; Wilson, J.; Millman, K. J.; Mayorov, N.; Nelson, A. R. J.; Jones, E.; Kern, R.; Larson, E.; Carey, C. J.; Polat, I.; Feng, Y.; Moore, E. W.; VanderPlas, J.; Laxalde, D.; Perktold, J.; Cimrman, R.; Henriksen, I.; Quintero, E. A.; Harris, C. R.; Archibald, A. M.; Ribeiro, A. H.; Pedregosa, F.; van Mulbregt, P. SciPy 1.0 Contributors. SciPy 1.0: fundamental algorithms for scientific computing in Python. *Nat. Methods* **2020**, *17*, 261−272.

(32) van der Walt, S.; Colbert, S. C.; Varoquaux, G. The NumPy Array: A Structure for Efficient Numerical Computation. *Comput. Sci. Eng.* **2011**, *13*, 22−30.

https://dx.doi.org/10.1021/acs.iecr.0c04414
Ind. Eng. Chem. Res. 2020, 59, 19999−20010

(33) Román, A. M.; Dudoff, J.; Baz, A.; Holewinski, A. Identifying "Optimal" Electrocatalysts: Impact of Operating Potential and Charge Transfer Model. *ACS Catal.* **2017**, *7*, 8641−8652.

https://dx.doi.org/10.1021/acs.iecr.0c04414
Ind. Eng. Chem. Res. 2020, 59, 19999−20010